JOURNAL OF THERMOPHYSICS AND HEAT TRANSFER
Vol. 21, No. 3, July–September 2007

Radiation Measurements in a Shock Tube for Titan Mixtures

Catherine Rond,* Pascal Boubert,† Jean-Marie Félio,‡ and Aziz Chikhaoui§
Université de Provence, 13013 Marseille, France

DOI: 10.2514/1.28422

Experiments have been carried out in the frame of the Huygens mission preparation to evaluate the radiative heat flux during the entry of the space probe into the atmosphere of Titan. Time-resolved emissions of CN and C_2 molecules are studied behind a strong shock wave generated in a free piston shock tube. CN violet, C_2 Swan, and CN red radiative systems are recorded for pressures from 40 to 1100 Pa at a shock velocity equal to 5500 m/s. The calibration of the emission measurement is carried out and values of absolute heat flux density are given. The calibrated time profiles are commented and the evolution with pressure of the nonequilibrium radiation is underlined. An analysis of the CN violet spectra is performed by comparison with a spectroscopic code, taking into account self-absorption and able to determine rotational and vibrational temperatures as well as ground state density by an iterative least-squares process. Last, obtained data led to the proportions of radiation emitted by CN violet and red systems as well as C_2 Swan bands.

Nomenclature

a_ν	=	absorption coefficient
D	=	diameter of the shock tube
i_ν	=	emission coefficient
L_ν	=	spectral intensity
p_i	=	initial pressure of mixture in the shock tube
p_s	=	postshock pressure
T_{exc}	=	electronic excitation temperature
T_r	=	rotational temperature
T_v	=	vibrational temperature
v_s	=	shock velocity
X_{CN}	=	molar fraction of CN molecule

I. Introduction

ON 14 January 2005, Huygens probe landed on the soil on Titan, the largest moon of Saturn. One thousand seconds before this successful landing, it had entered the atmosphere of Titan with a velocity greater than 6 km/s, meeting a mixture composed of about 97% of nitrogen, 2% of methane (the methane concentration increases up to 5% as the altitude decreases), and 1% of various species such as ammoniac, argon, and cyanhydric acid. Using aerodynamic braking on the dense layers of the upper atmosphere to reduce its velocity before opening its parachutes, Huygens and its heat shield received a large radiative flux whose maximum value occurred for an altitude of about 500 km where the atmospheric pressure is close to 15 Pa. The velocity of the probe was then 5.1 km/s.

Such a hypersonic velocity generates the formation of a bow shock in front of the heat shield of the space probe. In the shock layer, physical and chemical phenomena produce a nonequilibrium situation giving birth to a strong radiative emission from the excited species.

It is now well known that in those experimental conditions main radiative systems are C_2 Swan bands, the CN red system, and especially the CN violet system. CN and C_2 are produced behind the shock where CH_4 is strongly dissociated [1]. The knowledge of CN and C_2 formation kinetics as well as interaction between chemical kinetics and radiation are then of capital interest for future Titan missions but also for incoming missions to Mars and Venus. Large uncertainties remain in the way CN excited states are produced: directly from chemical reactions or by collisional excitation of the CN ground state. Currently, no model is able to predict a CN emission absolute value and time profile with a satisfactory agreement. Nelson's model [1] has been widely used especially during the design of the Huygens probe, but recently Gökçen [2] proposed a new chemical kinetic model gathering the most up-to-date data. Compared to Nelson's model, this model predicts lower CN number density and temperatures as well as a significantly different evolution of the electron number density.

Several experimental and computational studies have been performed since the last 15 years as mentioned in the comprehensive review given by Bose et al. [3] in their last work on the subject. These authors from the NASA Ames Research Center carried out some experiments in an electric arc shock tube for initial pressure equal to 13.3 and 133 Pa and shock velocity included in the 5–6 km/s range in N_2–CH_4 mixtures. Previously Labracherie et al. [4] and then Ramjaun et al. [5] carried out some experiments in a TCM2 free piston shock tube in Marseilles for an initial pressure equal to 200 Pa and a shock velocity equal to 5.6 km/s in N_2–CH_4 and N_2–CH_4–Ar mixtures. At the beginning of the 1990s, Park [6] and Park and Bershader [7] had carried out some experiments in a combustion driven shock tube at Stanford University for an initial pressure equal to 266 Pa and a shock velocity equal to 5.75 km/s in a N_2–CH_4–Ar mixture. All those authors obtained time-resolved emission of a CN violet system thanks to fast photomultipliers or streak cameras. Moreover, Bose et al. [3], on the one hand, and Park and Bershader [7], on the other hand, performed calibrated measurements.

The purpose of the present study is to estimate experimentally the radiative flux during an entry into the Titan atmosphere prior to the Huygens mission, on the one hand, and to complete previous studies, on the other hand. The presented results have been obtained by carrying out some experiments in the TCM2 free piston shock tube for initial pressures close to 40, 200, and 1100 Pa and a shock velocity around 5.5 km/s. Because the emphasis is on the radiative flux measurements, a streak camera has been used to obtained time evolution of the emission at different wavelengths corresponding to the three main radiative systems as well as spectral profiles of those systems at different times behind the shock. This technique brings

Presented as Paper 3240 at the 37th AIAA Plasmadynamics and Lasers Conference, San Francisco, California, 5–8 June 2006; received 18 October 2006; revision received 21 January 2007; accepted for publication 22 January 2007.

*Ph.D. Student, Department of Chemical Kinetics and Radiation, 5 rue Enrico Fermi; rond@polytech.univ-mrs.fr. Student Member AIAA.

†Assistant Professor, Department of Chemical Kinetics and Radiation, 5 rue Enrico Fermi; boubert@polytech.univ-mrs.fr. Member AIAA.

‡Engineer, Department of Chemical Kinetics and Radiation, 5 rue Enrico Fermi; felio@polytech.univ-mrs.fr.

§Professor, Department of Chemical Kinetics and Radiation, 5 rue Enrico Fermi; aziz@polytech.univ-mrs.fr.

data about the emitting species and more exactly on their excited states, though autoabsorption also allows probing ground state populations through emission measurements. To obtain absolute values of the heat flux density, streak images have been calibrated by comparison with the emission of a blackbody-simulating device. Calculation of CN violet spectra has been performed to extract vibrational and rotational temperatures as well as CN number density by taking into account self-absorption. Last, absolute measurements of the heat flux density performed on a narrow range of wavelength (one vibrational manifold) have been extrapolated to the whole systems thanks to the spectral simulation. Then, the respective ratios of emission of the CN violet system, C_2 Swan bands, and CN red system have been calculated.

II. Experimental Setup: TCM2 Wind Tunnel and Shock Tube

The experiments have been performed in a shock tube facility located at the University of Provence in Marseilles (France). TCM2, the shock tube facility, was initially built in the beginning of the 1990s in the frame of the Hermes program to be a powerful and clean wind tunnel for tests in air. TCM2 is a semi-industrial facility that requires constant preparation and maintenance by a team composed of at least three persons. In these conditions it is possible to carry out two or three runs a day.

The TCM2 wind tunnel is made according to the Stalker principle: a free piston (35 kg) hurled by high-pressure air continuously compresses a mass of helium. The increase of the pressure in helium (adiabatic compression) induces the breaking of a metallic membrane and the propagation of compression waves in the shock tube (diameter: 70 mm) filled with the test gas. The compression waves converge to a shock wave that can be optically studied through a test section equipped with quartz windows. At the end of the shock tube, the gas may be expanded through a conical nozzle to produce a hypersonic flow in a large test chamber where scaled models may be placed to study the recompression. Alternatively, the gas may be evacuated in a dump tank through a cylindrical section in the case of a shock wave study. This is the method that we used and this configuration is shown on Fig. 1.

All along the shock tube, pressure and temperature gauges allow one to locate the shock wave during the run and then to measure the shock velocity. Within this study, shock velocity was monitored using five pressure gauges located on the optical section (window) and 550, 750 and 1150 and 2900 mm before this point. Three temperature gauges located between the pressure gauges confirm the velocity measurement. The size of the gauges induces an uncertainty on the velocity measurements that remains lower than 40 m/s that corresponds to 0.72% of the nominal velocity met in the present study.

In wind tunnel configuration, different studies have been carried out on the expansion flow and on the bow shock around a cylindrical or spherical metallic model to determine the physical characteristics of the flow as well as its cleanness by a spectroscopic method [8]. Laser-induced fluorescence [8] and Raman scattering experiments [9] have also been carried out. In spite of its remarkable cleanness and considering the aerodynamic performance, TCM2 is now much less powerful for aerodynamic studies, but also much less expensive than big wind tunnels such as HIEST in Japan, facilities at GASL and Caltech in the USA, T4 in Australia, or HEG in Germany. On the contrary, it remains a high performance shock tube able to produce Mach numbers close to 25 in many gases. Indeed, it has been very early used as a shock tube for studies in Titan and Mars mixtures, and CO [4,5].

III. Measurement Techniques

A. Time-Resolved Emission Spectroscopy

Whereas laser spectroscopy and absorption spectroscopy give information about ground and low-energy states, emission spectroscopy is related to the excited states of the studied species and is especially interesting for determination of the radiative heat flux. Moreover, a comparison of the obtained spectra with calculated ones brings data such as vibrational temperature (or vibrational distribution in the case of vibrational nonequilibrium), rotational temperature, upper level number densities, and lower level number densities when self-absorption is no longer negligible.

Moreover, time-resolved spectroscopy, especially useful in one-run applications such as shock tube experiments, provides information about evolution of the emission with time (and then evolution of the parameters mentioned previously). It can be achieved by means of a streak camera. Coupling a spectrometer and a streak system allows one to obtain a time spectral picture for each run of the shock tube and to obtain spectral and time distribution of the radiation behind the shock wave. The time evolutions of parameters such as temperatures and densities are of great interest to validate chemical kinetic codes.

TCM2 is initially a wind tunnel and has been built for measurement on a model at the exit of the nozzle. The Stalker system generates recoil of the facility that induces a displacement of the tube during a test. Hence, the emission has to be collected through an optical fiber (high grade fused silica, transmittance equal to 0.55 from 260 nm to 2.2 μm) on which is focused the light coming through a 500 μm slit. The role of this slit is to ensure an acceptable space resolution. The optical setup is then verified before and after each test and is shown in Fig. 2.

Run-to-run uncertainties with the same initial conditions are close to 10% in terms of pressure and 20% in terms of species densities [8], which is expected in this kind of facility. Our absolute emission measurements show a run-to-run uncertainty equal to 25%. This uncertainty may be explained, on one hand by the effect of the intrinsic reproducibility on the temperatures behind the shock wave, and on the other hand by the relative moving of the collection system in regard to the shock tube during its recoil. However the run-to-run uncertainty on the relative results as the shape of the time and spectral profiles is close to 10%.

The window is made of UV fused silica whose transmittance is constant and equal to 0.92 from 200 nm to about 2 μm. This transmittance is taken into account during the postprocessing and the calibration process.

The entry slit aperture of the monochromator was 200 μm for CN violet, 500 μm for C_2 Swan, and 1500 μm for CN red. The Jobin–Yvon HR640 monochromator has been used with a 2400 grooves/mm grating for near UV measurements and with a 600 grooves/mm grating for visible measurements. The spectral resolution observed does not allow distinguishing the fine rotational

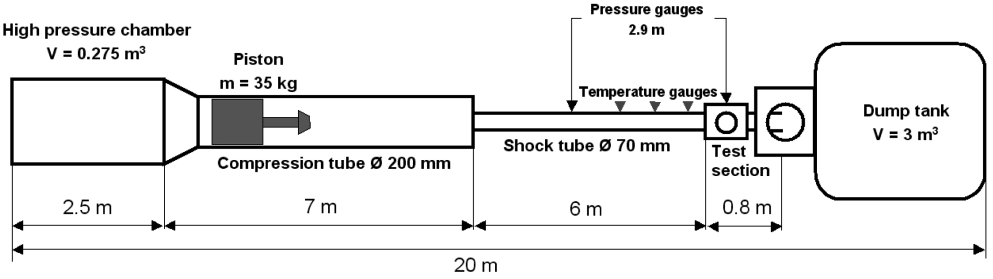

Fig. 1 TCM2 shock tube geometry and characteristics.

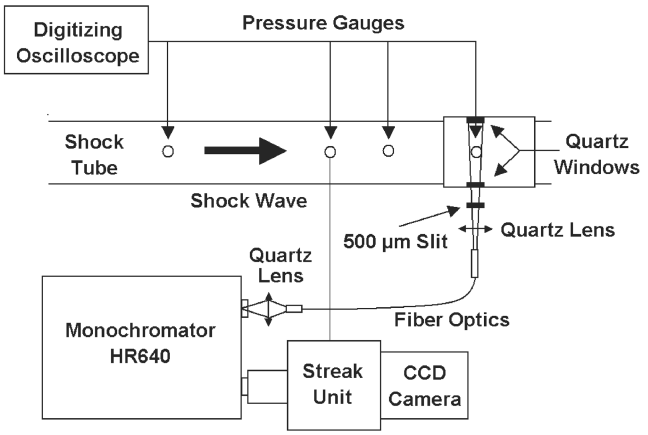

Fig. 2 Time-resolved emission spectroscopy optical setup.

structure of the spectra; however the rotational temperature has also a significant influence on its general shape. For measurements on the CN red system a frequency low-pass filter is placed between the monochromator and the streak camera to absorb the second-order of CN violet emission.

The streak system (Hamamatsu M1953 + C1587) is able to work with time ranges from 10 ns to 50 ms. Considering the characteristic duration of the studied phenomena, 20 and 200 μs time ranges have been used to capture the whole phenomenon with a good time resolution. The entry slit of the focusing optics of the streak system has been opened at 20 μm for CN violet measurements, 40 μm for C_2 Swan measurements, and 100 μm for CN red measurements. For low slit apertures used on the streak system within this study, the time resolution is just a function of the optical collection system (mainly of the width of the collection slit). It is close to 1 μs whatever the time range used. The streak camera is triggered by the signal given by one of the four pressure gauges upstream from the test section (also used to measure the shock velocity) through a delay generator. The choice of the gauge used for the trigger depends on the expected shock velocity and on the time range of the streak camera.

The spectral sensitivity of the system allows using it for measurements between 300 and 900 nm with good efficiency. Figure 3 gives an example of a time spectral image; the companion software presents the image in false colors but it is reproduced here in gray scale. The emission upstream from the shock wave may be due to photoexcitation or electroexcitation, but mainly to the reflection on the wall of the shock tube. Spectral and time profiles have been added on the top and on the right of the streak image, respectively. In this picture, the location of the dynamic shock is quite arbitrary. No measurement of the incubation time is carried out with a sufficient accuracy. Indeed, because of the size of the pressure gauges (5 mm), the uncertainty on the absolute shock time is greater than the incubation time. This incubation time corresponds to the temperature

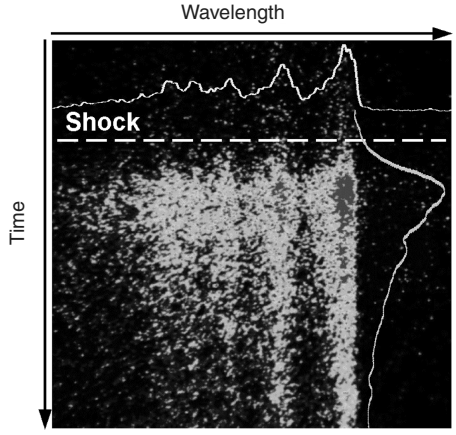

Fig. 3 Time spectral image of the CN violet emission. The range of wavelength is 383–391 nm and the time range is 20 μs.

increase, to the formation of radicals, and to the excitation of those molecules within the hypothesis where molecules are produced on ground states.

B. Calibration: Heat Flux Measurements

Attempts have been made to measure the heat flux emitted behind the shock wave by using a flux meter from ultraviolet to midinfrared with the help of filters. However, the bursting of the membranes as well as the braking of the piston induces a very high level of acoustic noise and mechanical vibration of the facility and the tests had been unsuccessful.

So, the optical setup has been calibrated in spectral intensity by means of a blackbody-simulating device used as a quasipunctual source. This apparatus is made of a tungsten disk heated in a conical furnace. Such a calibration has to provide an estimation of the radiative flux especially around 400 nm. However, such a method is not without difficulty and calibration problems are numerous:

1) The emission of the calibration device (2859 K) is not of the same order of magnitude as the emission of the medium behind the shock wave at the corresponding wavelengths. So a different time scale is used during calibration.

2) The blackbody is a Lambertian source while the medium is quite an isotropic source.

3) The emitting medium is not a punctual source since the diameter of the shock tube is 70 mm (measurements are made on the axis), and the collection system is set close to the source to keep a sufficient signal-to-noise ratio.

4) The numerical aperture of the optical fiber has to be taken into account.

5) Reflections on the wall of the tube are difficult to be estimated and induce a supplementary uncertainty.

Because the geometry of the effective medium and the geometry of the calibrating device are different, the light paths are different in both cases. To obtain an absolute value for the flux density emitted by the medium behind the shock wave, a direct simulation Monte Carlo (DSMC) calculation has been performed whose purpose is to determine the energy collected by the optical setup during the calibration tests and the effective emitting surface of the blackbody.

By fixing most of the issues, the remaining relative uncertainty on the calibration process may be estimated. The uncertainty on the calibrated values is estimated to $-67\%/+26\%$ which is mainly due to the weak depth of the field of the optical setup. In spite of this uncertainty the calibration process provides a maximum value for the heat flux. Moreover, the calibrated values on the equilibrium plateau are in good agreement with equilibrium calculations whatever the initial pressure condition. That means the effective error bars are certainly much lower that those predicted by the theoretical calculation.

IV. Data Processing

A. Image Postprocessing

The charge-coupled device (CCD) picture (background corrected by the camera software) is available in an ASCII format as a 1000×1018 matrix. Each point of the matrix is spotted by its two pixel coordinates and its value is given as an integer recorded on 12 bits (4096 levels). Spectra and time profiles are extracted and processed by a dedicated FORTRAN code. The code realizes the spectral and time calibration of the images as well as corrections needed to obtain absolute value of the energy received by each pixel: spectral sensitivity, camera gain, Lambertian/isotropic adjustment, slit width, solid angle, and calibration ratio.

B. Spectrum Calculations

Even if only the CN violet (B-X) system has been deeply investigated within this study, it was necessary to know the spectral distribution of the two other observed systems: CN red (A-X) system and C_2 Swan (d-a) bands. In the same way, possible perturbing systems, such as CH A-X, B-X, and C-X systems and the CN LeBlanc (B-A) system have also been considered in calculations.

A code has been developed to calculate the whole spectrum from 100 to 1200 nm with good accuracy. Toward this purpose, no hypothesis has been made on the energy level of CN and C_2; especially vibronic term values and rotational constants obtained from experiments when they were available have been preferred to Dunham expansion. Where experimental data were not available, constants have been extrapolated under the control of the physical meaning of the results. The doublet structure of $X^2\Sigma^+$, $A^2\Pi$ and $B^2\Sigma^+$ level of CN and the triplet structure of $d^3\Pi_g$ and $a^3\Pi_u$ of C_2 have been calculated as well as the fine structure. Such accuracy seems in opposition to the quite low resolution of the spectra recorded (close to 0.1 nm). Nevertheless, past studies on CN and C_2 showed that the general shape of the CN and C_2 spectra are sensitive to the rotational structure of the implied levels [10].

For the CN violet system, the matrix elements for the $^2\Sigma$ Hamiltonian given by Douay et al. [11] along with the recent vibrational and rotational constants of Ram et al. [12] have been used for energy calculations.

For the CN red system, the code refers to the paper of Kotlar et al. [13] for energy expressions as well as for constants.

For the CN LeBlanc system, we used constants from Prasad et al. [14] for A and B states.

For the C_2 Swan bands, the effective Hamiltonian of Brown and Merer [15] is diagonalized and used with the constants of Prasad and Bernath [16] for vibrational levels lower than 3 on the upper electronic state and 4 on the lower electronic state. For the upper vibrational level, the old model from Budó [17] is used along with the works of Phillips and Davis [18,19].

For the CH systems, data from Zachwieja [20] and from Luque and Crosley [21,22] have been used.

Rotational transition probabilities are calculated according to Kovács [23] with the corresponding summation rule. For the CN violet system, vibrational transition probabilities are taken from the paper of Knowles et al. [24]. Calculations have also been carried out with the vibrational transition probabilities computed by Lino da Silva [25] and Laux [26]. The influence of those different sources on the results extracted from the computed spectra is much lower than the experimental uncertainties. For the CN red system, the values determined by Laux [26] have been used. For the C_2 Swan bands, vibrational transition probabilities have been recalculated from the dependence of the electronic transition moment with the first r-centroïd moment established by Danylewych and Nicholls [27,28]; Franck–Condon factors are also given in this paper.

Although it is still under development, the code is also capable of calculating the radiation from atoms and most of the systems of the diatomic molecules present in the planetary atmosphere. Its results have been validated on spectra obtained in flames and plasma jets.

Considering the pressures behind the shock wave (from 2×10^4 to 3×10^5 Pa), self-absorption has to be considered in the calculations. Our radiative code is called to compute emission and absorption coefficient but also to rebuild experimental spectra. However, because of the simple geometry of the facility, the radiative transfer equation may be solved along the line of sight. Moreover, in a first approximation we neglected the boundary layer thickness and we considered that the radiative medium was homogeneous. The validation of those hypotheses and the determination of the evolution of the boundary layer thickness along the tube are under investigation through calculations carried out by M.-C. Druguet in the IUSTI laboratory. Considering this simple case, the radiative transfer equation is solved analytically:

$$L_\nu = \frac{i_\nu}{a_\nu}[1 - \exp(-a_\nu \cdot D)]$$

The code deals with pressure and Doppler broadenings and then with a Voigt line shape. The numerical spectral resolution has to be high enough to correctly describe the line shape. We show that in the near-ultraviolet and visible ranges, a resolution equal to 1000 points/nm is sufficient.

Evaluation of rotational and vibrational temperatures when they exist is achieved by point-to-point comparison between the experimental spectrum with calculated spectra by a least-squares method. The apparatus function (experimental spectral resolution) may also be taken as a free parameter although it is also determined experimentally. The value obtained by the minimization method is in agreement with the experimental value that is 0.12 nm (±0.02 nm) with a Gaussian shape. As said before, such a resolution does not allow observing the rotational structure of the spectra but nevertheless an estimation of the rotational temperature based on the shape of the vibronic bands is possible. The uncertainty of this determination is about 1000 or 500 K in regards to the signal-to-noise ratio. Conversely, the vibrational structure of the spectra is apparent and the determination of the vibrational temperature is based on the sensitivity of the band intensity to the vibrational temperature. Considering the quality of the spectra obtained and the overlapping of vibronic bands occurring in the CN violet system, the uncertainty on vibrational temperature measurements remains included between 500 and 1000 K. The vibrational temperature asks to be validated on several vibrational manifolds. Whatever the complexity of the spectra, the main source of uncertainty remains a low signal-to-noise ratio. Moreover, if the assumption of rotational equilibrium with translation is generally admitted, the existence and definition of a vibrational temperature may be argued especially in the nonequilibrium area. However, in contradiction with Ramjaun et al. [5] no strong vibrational nonequilibrium has been found and we considered the existence of the vibrational temperature in all cases.

V. Test Conditions

The different tests carried out may be gathered in three groups corresponding to three kinds of initial pressure with quite a constant velocity. Those three test conditions are presented in Table 1 with initial pressure (measured), postshock pressure (calculated), and shock velocity (measured). The values presented are some averages over the whole set of tests realized.

For both lower pressure conditions, experiments have been carried out for four different mixtures with variable proportions of nitrogen, methane, and argon. Those compositions correspond to the three Yelle profiles [29] and to a Titan-like mixture used in TCM2 for previous tests [4,5]. They are presented in Table 2. For the highest-pressure condition, tests have only been carried out in the TCM2 classical mixture. All the tests have been carried out before Huygens successful entry and to the latest determination of Titan atmosphere composition.

The purpose followed by varying the relative proportions of argon and methane in nitrogen in the mixture was to quantify their influence on the radiative flux and to complete the works of Labracherie et al. [30] on the influence of argon by quantitative values.

Because TCM2 is made to work with pressure close to a few tenths of atmospheric pressure, there is a prefilling uncertainty on the initial pressure in the shock tube that is independent of the pressure level

Table 1 The three test conditions. Postshock pressures are obtained thanks to the classical Rankine–Hugoniot equations applied to the shock front

p_i, hPa	p_s, hPa	v_s, km/s
11	3000	5.3
2	800	5.5
0.45	200	5.5

Table 2 Composition of studied mixture in %. For each molecule the second column gives the results of the analysis made by the gas manufacturer

	CH_4	Ar	N_2
TCM2 classical	3 (*2.96*)	5 (*5.02*)	92 (*92.02*)
Yelle nominal	3 (*2.93*)	2 (*2.15*)	95 (*94.92*)
Yelle minimal	5 (*5.06*)	0	95 (*94.96*)
Yelle maximal	1 (*1.00*)	10 (*10.30*)	89 (*88.70*)

and equal to 8 Pa. The postfilling uncertainty on this pressure is about 1 Pa. The relative uncertainties on the composition of the mixture are reduced to those given by the manufacturer and are lower than 2%. Because of a low leakage rate (lower than 10^{-1} Pa/ min when pressure is lower than 10^{-1} Pa), there is no significant contamination of the mixture present in the tube by outside air.

VI. Time Analysis

Time profiles are extracted from images by the postprocessing code summing the energy received over several horizontal pixels that is over a range of wavelength. This range may be the whole measurement window or may correspond to a vibrational band to obtain the time evolution of each vibrational level in case of vibrational nonequilibrium. But, considering the spectral resolution and the strong overlapping of vibrational bands, it remains difficult to obtain the time evolution of one vibrational band. So, time profiles presented are integrated over the specified range of wavelengths.

The beginning of the overshoot on the time profiles corresponds to the beginning of emission of the excited species. Formation and excitation of molecules and atoms need a few tenths of microsecond (incubation time) so the origin of the time as it is shown on the plots corresponds to the radiative shock. The incubation time depends of course of the scheme of CN and C_2 formation and excitation; this point remains a very relevant but unresolved issue. No direct measurement of the run of the shock wave through the optical axis is made with sufficient accuracy to determine the time corresponding to the jump of pressure and translation temperature.

It is important to remember that emission measurements are made perpendicularly to the move of the shock wave so that we have a look at the flux that is radiated at some distance (or some time) behind (or after, respectively) the shock wave. For this reason, the axes in our plots are scaled with a laboratory time different from a fluid time. Of course there is a relation between the laboratory time and the physical distance behind the shock wave but it requires knowing the fluid velocity behind the shock. For comparison with experiments giving the radiative flux in regards to the distance behind the shock wave (for example, when the whole shock layer is recorded thanks to an intensified camera [3]), we need to know the evolution of the flow velocity behind the shock wave. This velocity may be given by a classical calculation. Concerning the vertical axis, we chose to express the radiative power as a flux density in $W \cdot m^{-2} \cdot sr^{-1}$.

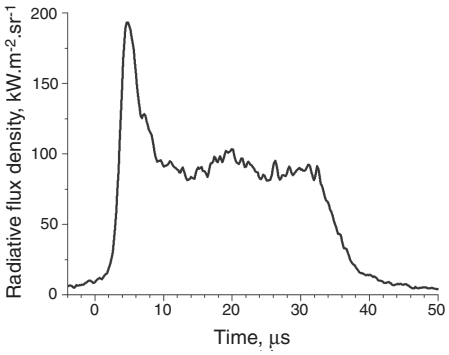

Fig. 4 Time evolution of the radiative flux from the CN violet system ($\Delta v = 0$). Yelle nominal mixture, $p_i = 210$ Pa, $v_s = 5620$ m/s.

The time profile shown in Fig. 4, as all the time profiles presented in this paper, shows an emission overshoot corresponding to the nonequilibrium status of the medium followed by an emission plateau corresponding to the equilibrium. The emission vanishes when the driver gas/test gas interface (contact surface) crosses the optical axis.

Because of the time resolution (fixed by the optical collection system) which is close to 1 μs, the rise of emission following the shock is not as sharp as could be expected from results of existing chemical kinetic codes which predict a rise time close to 0.2 μs for excitation temperature and CN number density.

Time profiles shown in Fig. 5 correspond to three tests with an initial pressure close to 200 Pa and a shock velocity close to 5500 m/s. Considering the absolute value of the flux density and the shape of the profile it is not possible to come to a conclusion about a significant influence of argon on the emission of CN. Labracherie et al. [30] found that the higher the amount of argon, the smaller the decay time to reach equilibrium. This phenomenon does not appear clearly in our results: in each case equilibrium is reached after 8 μs, whatever the argon initial concentration. However, in our experiments methane concentration also varies and the influence of the relative proportion of argon and methane is not investigated here.

Experiments carried out with a broadband spectrometer allowed us to record the whole near ultraviolet and visible spectrum during one run. It showed that the CN violet system is the main radiator in this range of wavelength and that the other expected sources of radiation, especially CN on the red transitions and C_2 along Swan bands in the green part of the spectrum, are much lower.

Figure 6 shows a comparison between the emission time profile of the three radiative systems observed in this study, CN violet and red systems, and C_2 Swan bands for an initial pressure close to 50 Pa and a velocity of about 5500 m/s.

It also gives the value of the radiative flux density integrated over a range of wavelength corresponding to the dispersion of the grating in the monochromator and centered on the considered vibrational manifold:

1) from 383 to 390 nm for the CN violet system ($\Delta v = 0$);
2) from 482 to 538 nm for the C_2 Swan bands ($\Delta v = 0$);
3) from 685 to 735 nm for the CN red system ($\Delta v = +3$).

To extrapolate these radiative energies to the whole systems, it is necessary to get some data about temperatures and self-absorption. Indeed, the ratio of the sums of transition probabilities is not useful in the case where self-absorption is relevant. In the next section, the

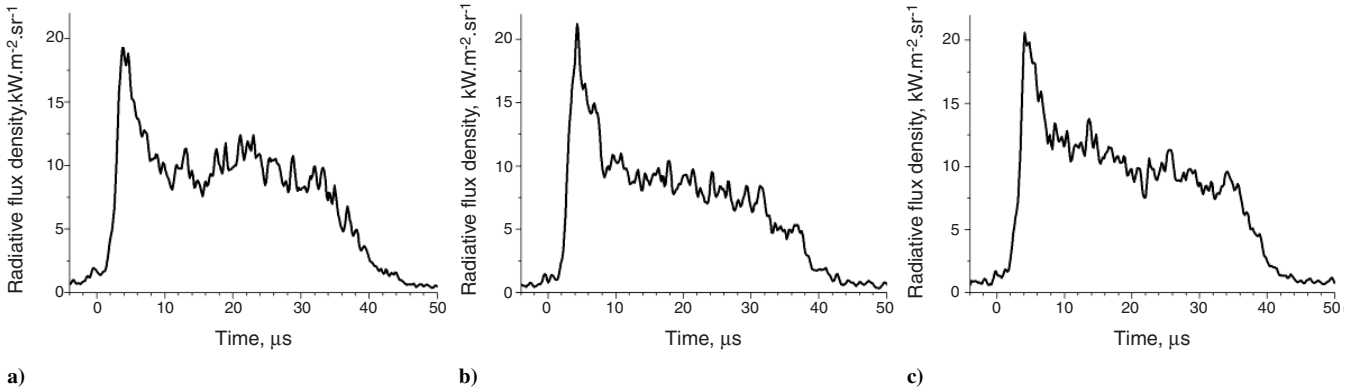

Fig. 5 Influence of mixture composition on the radiative flux from the CN violet system ($\Delta v = -1$). a) Yelle minimal mixture (argon 0%, methane 5%), $p_i = 210$ Pa, $v_s = 5500$ m/s; b) Yelle nominal mixture (argon 2%, methane 3%), $p_i = 205$ Pa, $v_s = 5580$ m/s; c) Yelle maximal mixture (argon 10%, methane 1%), $p_i = 200$ Pa, $v_s = 5600$ m/s.

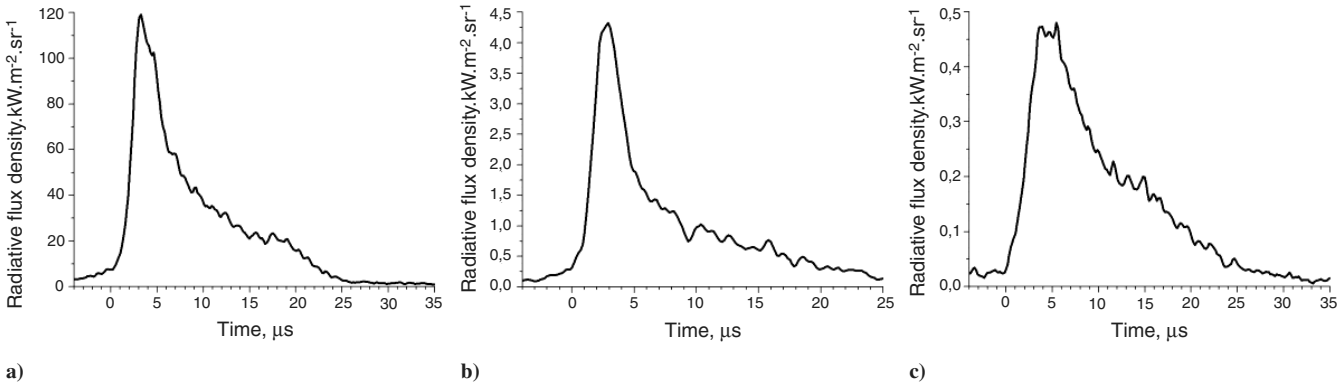

Fig. 6 Time evolution of the radiative flux in Yelle nominal mixture. a) CN violet system ($\Delta v = 0$), $p_i = 46$ Pa, $v_s = 5500$ m/s; b) C_2 Swan bands ($\Delta v = 0$), $p_i = 40$ Pa, $v_s = 5450$ m/s; c) CN red system ($\Delta v = +3$) $p_i = 46$ Pa, $v_s = 5580$ m/s.

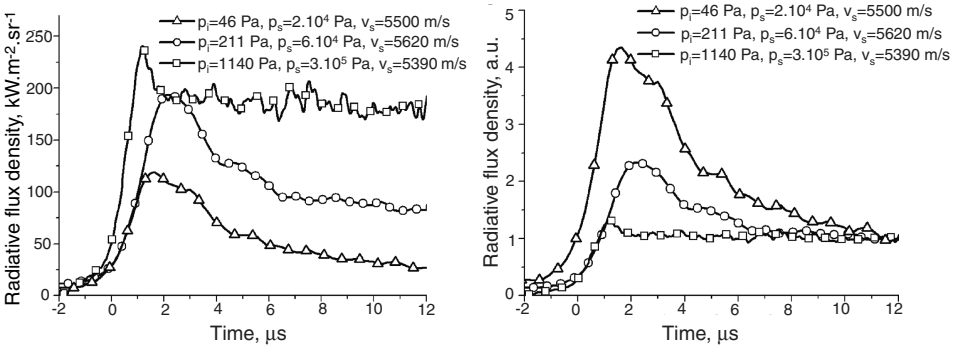

Fig. 7 Absolute (left) and normalized (right) time evolutions of the radiative flux from the CN violet system ($\Delta v = 0$) for the three kinds of pressures studied. Composition: 3% CH_4, 5% Ar, and 92% N_2.

spectral analysis of our results will give the needed data to carry out this extrapolation.

Figure 7 presents the absolute and normalized time profiles for the three pressure conditions. These two plots illustrate the two main pressure effects on the evolution on the emission behind the shock front. The absolute plot shows clearly that the total radiative flux density increases with the initial pressure of a gas test in the shock tube. However this increase is not linear because of self-absorption effects. The normalized plot emphasizes the difference between energy radiated during the nonequilibrium part and during the equilibrium part: the lower the initial pressure, the higher the nonequilibrium radiation. Let us notice the dependence of the time of experiment, which is limited by the driver gas/test gas interface (contact surface), with the pressure; the higher the pressure, the longer the time: 20 μs for an initial pressure $p_i = 45$ Pa, 35 μs for $p_i = 200$ Pa, and 60 μs for $p_i = 1100$ Pa. During the time of experiment, about one-third of the energy is radiated during the nonequilibrium phase for an initial pressure of 200 Pa. This ratio is very low for an initial pressure of 1100 Pa. On the contrary, for an initial pressure equal to 45 Pa, quite the whole amount of the radiated energy is emitted under nonequilibrium conditions because it is not sure that the CN B state (as well as the C_2 d state and CN A state) reaches equilibrium status before the end of the experiment. This behavior is illustrated in Fig. 8 where the ratio between the nonequilibrium peak and the equilibrium plateau levels has been plotted for a wide range of postshock pressures. Some points have been obtained on CN violet emission using mixtures other than Titan-like ones, especially mixtures containing CO and CO_2 [31].

Whatever the time for the excited states to be equilibrated, the radiative flux density in the equilibrium part is at least 10 times lower than at its maximum during the nonequilibrium phase. Very similar measurements carried out by Bose et al. [3] for pressures equal to 13.3 and 133 Pa in three different methane–nitrogen mixtures confirm this tendency but it is difficult to carry on with the comparison because the experimental conditions are different. Nevertheless the results of both studies are very coherent on this

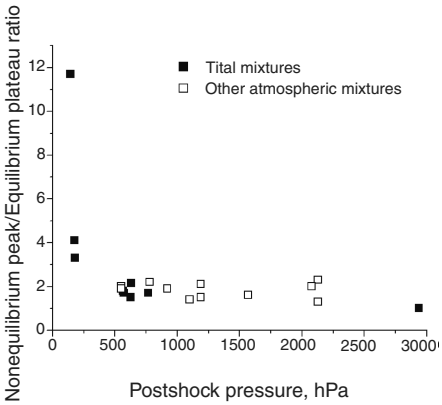

Fig. 8 Relative extent of nonequilibrium and equilibrium fluxes in regards to the postshock pressure.

issue, and that fact should be stressed. According to the trajectory, during the entry of Huygens in the atmosphere of Titan in January 2005, the velocity was close to 5.5 km/s for an ambient pressure of about 8 Pa. Considering a standoff distance equal to 10 cm [32], it is reasonable to assume that most of the radiative flux occurred in a nonequilibrium situation.

VII. Spectral Analysis

Spectra extracted from the images are obtained by the integration over a few pixels representing a few hundreds of nanoseconds. Although this process reduces significantly the time resolution of our analysis, it contributes to improve the quality and the physical meaning of our spectra and then the confidence in the extracted data. Quantitatively, spectral intensity can be expressed as a received energy density in $\mathrm{J \cdot m^{-2} \cdot nm^{-1} \cdot sr^{-1}}$ or as an average density of power by dividing by the time of integration; in this case the unit is

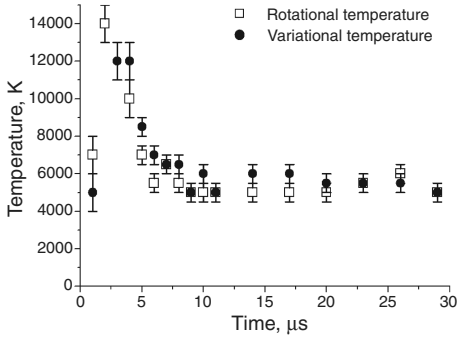

Fig. 9 Evolution of vibrational and rotational temperatures of the CN B state behind the shock wave. Yelle nominal mixture, $p_i = 210$ Pa, $v_s = 5620$ m/s. Composition: 3% CH_4, 2% Ar, and 95% N_2.

$W \cdot m^{-2} \cdot nm^{-1} \cdot sr^{-1}$. In the first time, spectra have been extracted each microsecond when the medium was considered out of equilibrium and each 3 μs when equilibrium was assumed. Spectral analysis has been carried out only on the violet system of CN that is the main radiative system. The lower resolution of the CN red and the C2 Swan spectrum does not give significant results. By comparing the obtained spectra with calculated ones to determine the best set of temperatures by an iterative process, the evolution of vibrational and rotational temperatures of the CN B state is obtained and is shown in Fig. 9 for an initial pressure equal to about 200 Pa. The uncertainty is equal to 1000 K in the nonequilibrium in the first 5 μs and to 500 K after 5 μs on both temperatures.

The results are in general agreement with what was expected from chemical kinetic calculations [1,3,32]. The agreement is especially good for the time evolution of CN violet radiation and for the temperatures, albeit calculations provide translational temperature and vibrational temperature of the ground states whereas our analysis conducts to rotational and vibrational temperatures of the excited B state of CN. On all the temperature profiles plotted, the same evolution of the vibrational temperature has been observed with a clear increasing above the equilibrium temperature in the first microseconds. Measurements have to be improved in the first 5 μs during the time where the gas is out of equilibrium. Two-temperature and multitemperature models, based on Rankine–Hugoniot initial conditions behind the shock predict an increase of the vibrational temperature and a decrease of the rotational/translational temperature thanks to vibration-translation exchange. However those temperatures, especially vibrational temperature, probably do not exist in the nonequilibrium area. Physical models need measurements of the vibrational distribution in the first microseconds after the shock to be validated especially for low initial pressure where nonequilibrium conditions are predominant. Similar plots have been performed for test with a lower pressure but the low signal-to-noise ratio leads to huge uncertainty that leaves the results unreliable.

Whereas most of our experiments have been calibrated in spectral intensity, older measurements carried out of $\Delta v = -2, -1$ and $+1$ of the CN violet system were not. Nevertheless an estimation of the ground state density of the studied species may be obtained from the analysis of the relative spectra when self-absorption is significant. Figures 10–13 present the comparison of experimental CN spectra on its four main vibrational manifolds with calculated spectra when equilibrium is assumed to be achieved, 2 μs after the shock. In the first time, vibrational and rotational temperatures, the CN number density and even the slit function had been left as free parameters. However, the influences of those parameters on the spectra are not independent and after all the slit function has been fixed to the experimental value and only one temperature has been considered because the four experimental spectra have been obtained by integration on the equilibrium part. In spite of the insufficient spectral resolution, rotational temperature remains a relevant parameter in the calculation and the resulting spectra are very sensitive to this parameter.

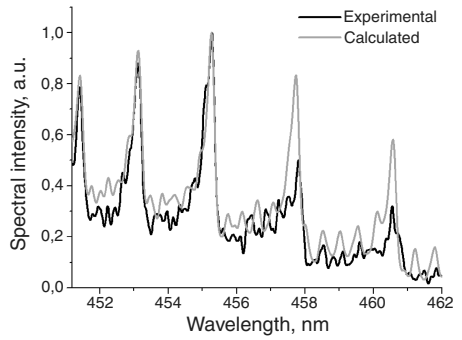

Fig. 10 Experimental and calculated spectra of the CN violet system ($\Delta v = -2$). Experiment: $p_i = 1009$ Pa, $v_s = 5320$ m/s. Calculation: $T_v = 5000$ K, $T_r = 5000$ K, low sensitivity to CN density. Composition: 3% CH_4, 5% Ar, and 92% N_2.

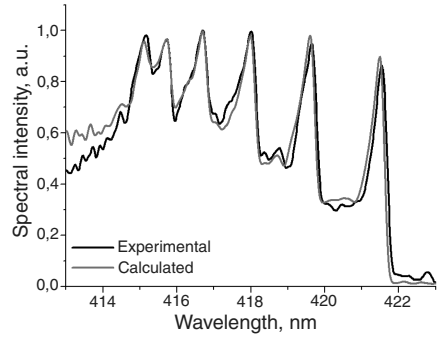

Fig. 11 Experimental and calculated spectra of CN violet system ($\Delta v = -1$). Experiment: $p_i = 1150$ Pa, $v_s = 5120$ m/s. Calculation: $T_v = 6000$ K, $T_r = 6000$ K, $Y_{CN} = 15 \times 10^{-3}$. Composition: 3% CH_4, 5% Ar, and 92% N_2.

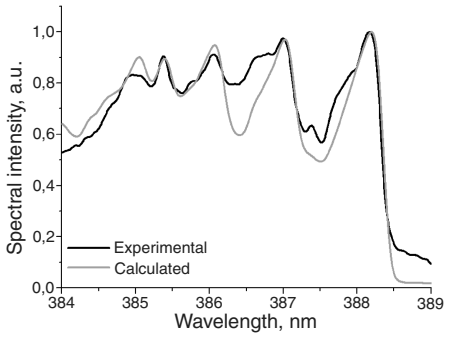

Fig. 12 Experimental and calculated spectra of the CN violet system ($\Delta v = 0$). Experiment: $p_i = 1092$ Pa, $v_s = 5380$ m/s. Calculation: $T_v = 6000$ K, $T_r = 6000$ K, $Y_{CN} = 2 \times 10^{-3}$. Composition: 3% CH_4, 5% Ar, and 92% N_2.

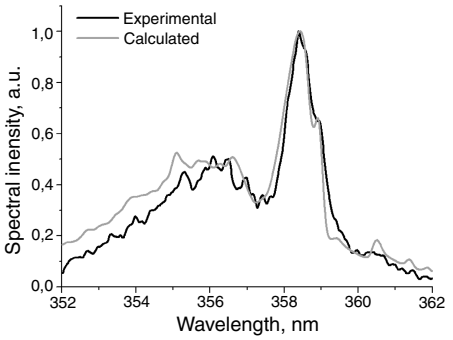

Fig. 13 Experimental and calculated spectra of the CN violet system ($\Delta v = +1$). Experiment: $p_i = 1154$ Pa, $v_s = 5076$ m/s. Calculation: $T_v = 6500$ K, $T_r = 6500$ K, $Y_{CN} = 5 \times 10^{-3}$. Composition: 3% CH_4, 5% Ar, and 92% N_2.

As pointed out in the legends of the figures, the four spectra have been obtained with close but different conditions. A quite good agreement is obtained on a temperature close to 6000 K and an average CN molar fraction equal to 5×10^{-3}. Discrepancies from these values cannot entirely be explained by the different initial conditions. Calculations show that a small variation of the initial pressure (lower than 10%) has a low effect on temperature and the CN molar fraction. Moreover a variation of 400 m/s on the shock velocity induced a variation of about 400 K on the equilibrium temperature and of 20% on the CN molar fraction. For a velocity of 5300 m/s and an initial pressure equal to 1000 Pa, such a calculation gives an equilibrium temperature equal to 6000 K and a CN molar fraction equal to 10^{-2}. In spite of the observed discrepancies, the uncertainty on the indicated temperatures and CN molar fraction is quite low because the shape of the CN violet spectra is very sensitive to those parameters. Determination of the temperature and the CN molar fraction is not independent and several couples of values may be found for the same spectrum. Nevertheless, a pessimistic estimation of the uncertainty on temperature gives 500 K and about 20% on the CN molar fraction (including CN violet $\Delta v = -1$ spectrum, CN violet $\Delta v = -2$ spectrum is not sensitive to self-absorption). In equilibrium conditions, the absolute calibration brings an estimation of the electronic excitation temperature that is found rather close to 6500 K while the spectrum fit quite well with a CN molar fraction close to 10^{-2}. However those last values remain an estimation because of the sums of run-to-run and calibration uncertainties. Let us notice that the signal-to-noise ratio is much lower for the CN $\Delta v = -2$ spectrum.

As written previously, we took into account a possible perturbation of the CN violet spectrum by CN LeBlanc and CH A-X, B-X, and C-X emissions. No significant perturbation by those systems has been pointed out. Spectral calculations show that in the present condition the CN LeBlanc system is 500 times lower than the CN violet system. Concerning CH, the absence of identifiable emission of its most radiative systems allows one to conclude that CH molar fraction remains lower than 10^{-3}.

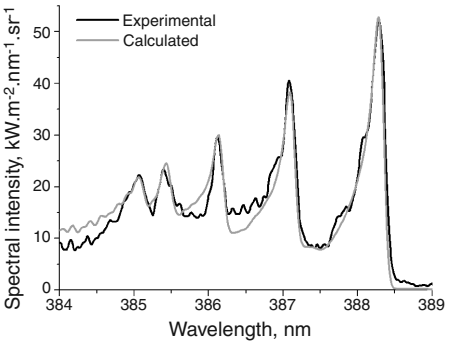

Fig. 14 Experimental and calculated spectra of the CN violet system ($\Delta v = 0$). Experiment: $p_i = 210$ Pa, $v_s = 5620$ m/s. Calculation: $T_v = 6000$ K, $T_r = 6000$ K, $T_{\text{exc}} = 7800$ K, $Y_{\text{CN}} = 8 \times 10^{-4}$. Composition: 3% CH_4, 2% Ar, and 95% N_2.

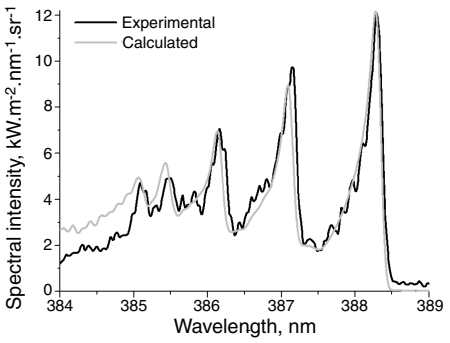

Fig. 15 Experimental and calculated spectra of the CN violet system ($\Delta v = 0$). Experiment: $p_i = 46$ Pa, $v_s = 5500$ m/s. Calculation: $T_v = 5500$ K, $T_r = 5500$ K, $T_{\text{exc}} = 5800$ K, $Y_{\text{CN}} = 3 \times 10^{-3}$. Composition: 3% CH_4, 2% Ar, and 95% N_2.

The same work has been realized for other pressure conditions. The results are shown in Figs. 14 and 15.

As for the high-pressure condition, the agreement between the results of the code and the experimental spectra is satisfying. Remaining discrepancies in the tail of the CN violet manifolds corresponding to high rotational levels might be explained by a lower rotational temperature that would not be coherent with our equilibrium hypothesis. Variations on the maximum rotation quantum number involved in the calculation do not give satisfying results.

Once the vibrational and rotational temperatures are determined along with the CN molar fraction assuming equilibrium, a comparison of the calibrated and computed spectral densities leads to the electronic excitation temperature. Considering the errors bars, it is in agreement with other temperatures for the lowest pressure case but much higher for the middle pressure conditions. This difference between apparent equilibrium temperature and estimated electronic excitation temperature is not explained either by the observed uncertainty or by the calculated uncertainty. This disagreement is quite disappointing because it should have been a reliable method to validate the calibration from the measurement temperatures. However it had been observed on every run in those operating conditions.

Because temperatures and CN number density are now estimated, it is possible to extrapolate the absolute values of spectral intensity obtained in a limited range of wavelength to the whole systems. For the test condition $p_i = 55$ Pa and $v_s = 5500$ m/s, which is the closest condition from the maximum radiative flux point of the Huygens entry trajectory, the spectral prediction code is able to calculate the following:

1) The ratio of CN violet ($\Delta v = 0$) intensity to total CN violet intensity that is equal to 0.54. That gives a total CN violet intensity equal to 184 $\text{kJ} \cdot \text{m}^{-2} \cdot \text{sr}^{-1}$.

2) The ratio of C_2 Swan ($\Delta v = 0$) intensity to total C_2 Swan intensity that is equal to 0.38. That gives a total C_2 Swan intensity equal to 8 $\text{kJ} \cdot \text{m}^{-2} \cdot \text{sr}^{-1}$.

3) The ratio of CN red ($\Delta v = +3$) intensity to total CN red intensity that is equal to 0.11. That gives a total CN red intensity equal to 5.5 $\text{kJ} \cdot \text{m}^{-2} \cdot \text{sr}^{-1}$.

Because spectral resolution was not sufficient to extract temperature from C_2 and CN red spectra, the previous calculation is made using the temperatures obtained on the CN violet spectrum. Most on the radiative energy being emitted under a nonequilibrium condition, the previous hypothesis has to be checked and the value given in this paper for C_2 and CN red contributions should be taken as an estimation. The CN red contribution found within this study is much lower than the contribution measured by Bose et al. [3], for instance. However, we observe that the lower the initial pressure, the higher the nonequilibrium and then the lower the contribution of CN red to the total flux.

Considering that those three systems are the only significant radiative systems between 300 and 1500 nm, the total energy density emitted during the time of experiment is very close to 200 $\text{kJ} \cdot \text{m}^{-2} \cdot \text{sr}^{-1}$ with 93% of CN violet, 4% of C_2 Swan, and 3% of CN red.

VIII. Conclusions

Radiative heat flux emitted behind a strong shock wave has been investigated at $v_s = 5500$ m/s for three initial pressure conditions (50, 200, and 1100 Pa) and for various compositions of Titan-like mixtures.

Time-resolved emission spectroscopy allowed an analyzing time evolution of CN violet emission and rotational and vibrational temperatures from the shock to the thermochemical equilibrium. Comparison of experimental spectra with calculation taking into account self-absorption allowed the estimation of the CN number density. Calibration of the optical system produced absolute values of heat flux density. For one condition, the C_2 Swan and the CN red

system have also been investigated and absolute radiative energies emitted along the three systems have been compared. It showed that C_2 Swan bands and the CN red system remain weak emitters at low pressure compared to the CN violet system.

This work completes previous works [3–7] and stresses the need for absolute measurements with reliable accuracy and the need of data directly comparable to computation results. Among those data, vibrational temperatures of the ground states and number densities seem to be the first steps to achieve to understand chemical kinetics during the space probe entry phase. In this paper the emphasis is on the radiative flux measurements and the presented results have to be compared to calculations first based on a 1-D axisymmetric two-temperature model, and then to an Euler computation taking into account the boundary layer effect and including an improved physical model. Such experimental studies that focus on radiation should be completed by measurements of densities and temperatures of the ground states.

Existing experimental results plead for a development of optical diagnostics to get new data or to increase the accuracy on heat flux measurements as well as on density and temperature measurements. Techniques such as laser absorption but also laser-induced fluorescence have to be considered now to provide more exhaustive sets of results. Existing results also speak for parallel works on a pure chemical kinetic model to be compared with future experimental results and, because excitation processes are far from being understood, a more complex collisional-radiative model.

Acknowledgments

This work was funded by the Huygens program of the European Space Agency. The authors thank André Bois and Roland Redon from the Applied Optics Laboratory of the University of Toulon-Var for their help in the calibration of the optical collection system, as well as Franck Mazoué from AOES (Advanced Operation and Engineering Services) for the chemical kinetics calculations.

References

[1] Nelson, H. F., Park, C., and Whiting, E. E., "Titan Atmospheric Composition by Hypervelocity Shock Layer Analysis," AIAA Paper 1989-1770, 1989.

[2] Gökcen, T., "N_2-CH_4-Ar Chemical Kinetic Model for Simulations of Atmospheric Entry to Titan," AIAA Paper 2004-2469, 2004.

[3] Bose, D., Wright, M. J., Bogdanoff, D. W., Raiche, G. A., and Allen, G. A., "Modeling and Experimental Validation of CN Radiation Behind a Strong Shock Wave," AIAA Paper 2005-0768, 2005.

[4] Labracherie, L., Billiotte, M., and Houas, L., "Non-Equilibrium Determination of Temperature Profiles by Emission Spectroscopy," *Journal of Quantitative Spectroscopy and Radiative Transfer*, Vol. 54, No. 3, 1995, pp. 573–579.

[5] Ramjaun, D., Dumitrescu, M., and Brun, R., "Kinetics of Free Radicals Behind Strong Shock Waves," *Journal of Thermophysics and Heat Transfer*, Vol. 13, No. 2, 1999, pp. 219–225.

[6] Park, C. S., "Studies of Radiative Emission from the Simulated Shock Layer of the Huygens Probe,'' Ph.D. Thesis, Stanford University, Palo Alto, CA, 1991.

[7] Park, C. S., and Bershader, D., "Studies of Radiative Emission from the Simulated Shock Layer of the Huygens Probe," *Proceedings of the 18th International Symposium on Shock Waves*, Springer–Verlag, Berlin, 1992, pp. 671–676.

[8] Boubert, P., Chaix, A., Chikhaoui, A., Robin, L., and Vervisch, P., "Aerodynamic Calibration of TCM2 Facility and Study of a Bow Shock Later by Emission and Laser Spectroscopy," *Shock Waves*, Vol. 11, No. 5, 2002, pp. 341–351.

[9] Pilverdier, H., Brun, R., and Dumitrescu, M. P., "Emission and Raman Spectroscopy Measurements in Hypersonic Nitrogen Flows," *Journal of Thermophysics and Heat Transfer*, Vol. 15, No. 4, 2001, pp. 484–490.

[10] Boubert, P., and Vervisch, P., "CN Spectroscopy and Physico-Chemistry in the Boundary Layer of a C/SiC Tile in a Low Pressure Nitrogen/Carbon Dioxide Plasma Flow," *Journal of Chemical Physics*, Vol. 112, No. 23, 2000, pp. 10482–10490.

[11] Douay, M., Rogers, S. A., and Bernath, P. F., "Infrared Fourier Transform Spectroscopy of XeH," *Molecular Physics*, Vol. 64, No. 3, 1988, pp. 425–436.

[12] Ram, R. S., Davis, S. P., Wallace, L., Engleman, R., Appadoo, D. R. T., and Bernath, P. F., "Fourier Transform Spectroscopy of the $B^2\Sigma^+$-$X^2\Sigma^+$ System of CN," *Journal of Molecular Spectroscopy*, Vol. 237, No. 2, 2006, pp. 225–231.

[13] Kotlar, A. J., Field, R. W., Steinfeld, J. I., and Coxon, J. A., "Analysis of Perturbations in the $A^2\Pi$-$X^2\Sigma^+$ 'Red' System of CN," *Journal of Molecular Spectroscopy*, Vol. 80, No. 1, 1980, pp. 86–108.

[14] Prasad, C. V. V., and Bernath, P. F., "Fourier Transform Jet-Emission Spectroscopy of the $A^2\Pi_i$-$X^2\Sigma^+$ Transition of CN," *Journal of Molecular Spectroscopy*, Vol. 156, No. 2, 1992, pp. 327–340.

[15] Brown, J. M., and Merer, A. J., "Lambda-Type Doubling Parameters for Molecules in Π Electronic State of Triplet and Higher Multiplicity," *Journal of Molecular Spectroscopy*, Vol. 74, No. 3, 1979, pp. 488–494.

[16] Prasad, C. V. V., and Bernath, P. F., "Fourier Transform Spectroscopy of the Swan $d^3\Pi_g$-$a^3\Pi_u$ System of Jet-Cooled C_2 Molecule," *Astrophysical Journal*, Vol. 426, No. 2, 1994, pp. 812–821.

[17] Budó, A., "Über des Triplett-Bandentermformel für den Allge Meinen Intermediären Fall," *Zeitschrift für Physik*, Vol. 96, 1935, pp. 219–229.

[18] Phillips, J. G., "Perturbations in the Swan System of the C_2 Molecule," *Journal of Molecular Spectroscopy*, Vol. 28, No. 2, 1968, pp. 233–242.

[19] Phillips, J. G., and Davis, S. P., "The Swan System of the C_2 Molecule," University of California—Berkeley and Los Angeles, Technical Rept., 1968.

[20] Zachwieja, M., "New Investigations of the $A^2\Delta$-$X^2\Pi$ Band System in the CH Radical and a New Reduction of the Vibration-Rotation Spectrum of CH from the ATMOS Spectra," *Journal of Molecular Spectroscopy*, Vol. 170, No. 2, 1995, pp. 285–309.

[21] Luque, J., and Crosley, D. R., "Electronic Transition Moment and Rotational Transition Probabilities in CH. I. $A^2\Delta$-$X^2\Pi$ System," *Journal of Chemical Physics*, Vol. 104, No. 6, 1996, pp. 2146–2155.

[22] Luque, J., and Crosley, D. R., "Electronic Transition Moment and Rotational Transition Probabilities in CH. II. $B^2\Sigma^-$-$X^2\Pi$ System," *Journal of Chemical Physics*, Vol. 104, No. 6, 1996, pp. 2146–2155.

[23] Kovács, I., *Rotational Structure in the Spectra of Diatomic Molecules*, Adam Hilger Ltd., London, 1969.

[24] Knowles, P. J., Werner, H.-J., Hay, P. J., and Cartwright, D. C., "The $A^2\Pi$-$X^2\Sigma^+$ Red and $B^2\Sigma^+$-$X^2\Sigma^+$ Violet Systems of the CN Radical: Accurate Multireference Configuration Interaction Calculations of the Radiative Transition Probabilities," *Journal of Chemical Physics*, Vol. 89, No. 12, 1988, pp. 7334–7343.

[25] Lino da Silva, M., and Dudeck, M., "A Line-by-Line Spectroscopic Code for the Simulation of Plasma Radiation During Planetary Entries," AIAA Paper 2004-2469, 2004.

[26] Laux, C. O., "Optical Diagnostics and Radiative Emission of Air Plasmas," Ph.D. Thesis, Stanford University, Stanford, CA, HTGL Rept., 1993.

[27] Danylewych, L. L., and Nicholls, R. W., "Intensity Measurements on the C_2 $d^3\Pi_g$-$a^3\Pi_u$ Swan Band System. 1. Intercept and Partial Band Method," *Proceedings of the Royal Society of London*, Vol. 339, No. 1617, 1974, pp. 197–212.

[28] Danylewych, L. L., and Nicholls, R. W., "Intensity Measurements on the C_2 $d^3\Pi_g$-$a^3\Pi_u$ Swan Band System. 2. Interpretation of Band Intensity Measurements from Synthetic Spectra," *Proceedings of the Royal Society of London*, Vol. 339, No. 1617, 1974, pp. 213–222.

[29] Yelle, R. V., Strobell, D. F., Lellouch, E., and Gautier, D., "Engineering Models for Titan's Atmosphere," ESA SP-1177, European Space Agency, Noordwijk, 1997.

[30] Labracherie, L., Billiotte, M., and Houas, L., "Shock Tube Analysis of Argon Influence in Titan Radiative Environment," *Journal of Thermophysics and Heat Transfer*, Vol. 10, No. 1, 1996, pp. 162–168.

[31] Rond, C., Boubert, P., Félio, J.-M., and Chikhaoui, A., "Non-Equilibrium Radiation Behind a Strong Shock Wave in CO_2-N_2 Mixture: Experiment and Modeling," *Chemical Physics* (submitted for publication).

[32] Mazoué, F., "Flow-Field/Radiation Coupling Analysis for Huygens Probe Entry into Titan Atmosphere," AIAA Paper 2005-5392, 2005.